

Multi-frame Detection via Graph Neural Networks: A Link Prediction Approach

Zhihao Lin

National Key Laboratory of Radar Signal Processing, Xidian University, Xi'an, 710071, China

Chang Gao

National Key Laboratory of Radar Signal Processing, Xidian University, Xi'an, 710071, China

Junkun Yan

National Key Laboratory of Radar Signal Processing, Xidian University, Xi'an, 710071, China

Qingfu Zhang

Department of Computer Science, City University of Hong Kong, Hong Kong, 999077, China

Hongwei Liu

National Key Laboratory of Radar Signal Processing, Xidian University, Xi'an, 710071, China

Abstract— Multi-frame detection algorithms can effectively utilize the correlation between consecutive echoes to improve the detection performance of weak targets. Existing efficient multi-frame detection algorithms are typically based on three sequential steps: plot extraction via a relative low primary threshold, track search and track detection. However, these three-stage processing algorithms may result in a notable loss of detection performance and do not fully leverage the available echo information across frames. As to applying graph neural networks in multi-frame detection, the algorithms are primarily based on node classification tasks, which cannot directly output target tracks. In this paper, we reformulate the multi-frame detection problem as a link prediction task in graphs. First, we perform a rough association of multi-frame observations that exceed the low threshold to construct observation association graphs. Subsequently, the Multi-feature Link Prediction

This work was supported in part by Hong Kong Innovation and Technology Commission Funding Administrative System II (ITF Ref. No. GHP/110/20GD) and the National Natural Science Foundation of China (62192714, U21B2006). (Corresponding author: Hongwei Liu; Chang Gao.)

Authors' addresses: Zhihao Lin, Junkun Yan and Hongwei Liu are with the National Key Laboratory of Radar Signal Processing, Xidian University, Xi'an, 710071, China, E-mail: (zhihlin@stu.xidian.edu.cn; jkyan@xidian.edu.cn; hwliu@xidian.edu.cn). Chang Gao is with the National Key Laboratory of Radar Signal Processing, Xidian University, Xi'an, 710071, China, and was also with the Department of Computer Science, City University of Hong Kong, Hong Kong, E-mail: (chang-gao@xidian.edu.cn). Qingfu Zhang is with the Department of Computer Science, City University of Hong Kong, Hong Kong, and also with the City University of Hong Kong Shenzhen Research Institute, Shenzhen, 518057, China, E-mail: (qingfu.zhang@cityu.edu.hk). (Corresponding author: Hongwei Liu; Chang Gao.)

Network is designed based on graph neural networks, which integrates multi-dimensional information, including echo structure, Doppler information, and spatio-temporal coupling of plots. By leveraging the principle of link prediction, we unifies the processes of track search and track detection into one step to reduce performance loss and directly output target tracks. Experimental results indicate that, compared with traditional single-frame and multi-frame detection algorithms, the proposed algorithm improves the detection performance of weak targets while suppressing false alarms. Additionally, interpretable analysis shows that the designed network effectively integrates the utilized features, allowing for accurate associations between targets and false alarms.

Key Words— Multi-frame Detection, Graph Neural Network, Link Prediction, Weak Target Detection

I. INTRODUCTION

TARGET detection aims to determine whether a signal received by sensors originates from a target based on the signal strength[1]. Effective target detection serves as the foundation for subsequent operations such as target tracking and target recognition. The reliable detection of weak targets still remains a critical challenge that urgently needs to be addressed in systems such as radar and sonar. The traditional signal processing framework, which follows a sequential pattern of track after detection, struggles to balance detection performance with system processing load, and its drawbacks are particularly evident in weak target detection scenarios[2],[3],[4]. To address the shortcomings of traditional signal processing, multi-frame detection (MFD) methods leverage the regularity of target motion and the accumulation of target energy to correctly integrate the echo information along the unknown target trajectories in multiple frames, thereby suppressing false alarms while improving the detection performance for low signal-to-noise ratio (SNR) targets[5],[6],[7].

Traditional MFD methods enable the successful detection of weak targets by directly utilizing un-thresholded raw echo data, but they exhibit significant drawbacks in high-resolution detection scenarios that require a large number of detection units[8],[9],[10],[11],[12]. On one hand, the large volume of raw observations will impose a substantial computational burden on the system. On the other hand, the observation uncertainty introduced by excessive false alarms makes it difficult to correctly associate targets. Although some methods focus on improving the accuracy of target association in different scenarios, they still do not consider the possibility of pre-filtering the candidate detection set based on the strength of the received echoes[13],[14],[15],[16],[17]. A viable approach to address the aforementioned challenge is a type of search-before-detect MFD method, which typically involves three steps[18]: First, a relatively low primary threshold is set for detection and plot extraction on each frame, which aims to maintain good detection performance for weak targets while filtering out observations unlikely to originate from actual targets, thereby reducing computational load. Second, for multi-frame observations that exceed the low threshold, potential tracks are searched by leveraging target kinematic

constraints. Finally, a fusion decision is made along the potential tracks based on information such as echo energy. This kind of method transforms single-frame plot-level detection into multi-frame track-level detection, ensuring robust detection performance for weak targets without requiring successful detection in every frame. However, such sequential track search and track detection limit the overall performance by the effectiveness of the potential track search.

Traditional track search methods primarily rely on position and Doppler information to establish kinematic constraints[18],[19],[20],[21]. In MFD methods that incorporate neural networks, reference [22] adopts a search-before-detect approach, first performing track search based on the coupled position and Doppler measurements, then conducting track detection using a data-driven method that integrates multi-dimensional information[23]. Reference [24] extends the scenario to bistatic radar systems based on this concept. Nevertheless, the model-driven track search used in these methods often lead to target missed associations when there is a model mismatch. Because it is difficult to apply unified constraint parameters that can reliably associate targets with different kinematic features, which in turn hinders the track detection process.

Graphs, as a mathematical language in the physical world, can reasonably describe multi-frame data[25]. Compared to other neural network, graph neural networks (GNNs) are capable of modeling the data characteristics from both structural and functional perspectives, successfully extracting data features even with a limited number of labels[26],[27],[28],[29]. Although the sparse distribution of targets in the observation space results in a limited number of target labels, the use of GNNs can effectively address this shortcoming. In the detection methods which apply GNNs, reference [30] introduces a novel approach using GNNs to develop a message-passing solution for the inference task of massive multiple-input multiple-output (MIMO) detection in wireless communication. Reference [31] constructs graphs from point cloud data obtained from sensors in the field of autonomous driving, leveraging GNNs to fully exploit point features and relationship characteristics among points, achieving object detection and classification through a node prediction task. Reference [32], in a maritime scenario, similarly employs the node classification concept within GNNs to distinguish targets and clutter in multi-frame observations. However, this method cannot directly output target tracks based on node classification task and fails to incorporate domain knowledge to construct the features of edges.

To overcome the limitations of model-driven track search and achieve target detection in environments with dense false alarms, a data-driven approach should enhance the accuracy of target association [33]. The process of track detection from multi-frame observations can be viewed as a nonlinear mapping from multi-dimensional information to the determination of whether a trajectory originates from a target. Furthermore, the track search and

detection process is fundamentally equivalent to a clustering problem of spatio-temporal plot associations. Unlike the node classification in GNNs, link prediction within graphs can be utilized to integrate multi-dimensional features on different attributes, thereby accomplishing track search and detection in a unified manner[34],[35]. This approach allows for direct output of target trajectories from multi-frame observations, simplifying the processing logic while reducing the loss in track search, ultimately leading to improved target detection performance.

Based on the above considerations, we propose a multi-frame detection algorithm via graph neural network-based link prediction (GLP-MFD). The proposed algorithm first leverages prior knowledge of target kinematic to perform a rough association of consecutive multi-frame observations that exceed the low threshold, aiming to minimize target missed associations while constructing observation association graphs. The features like echo structure and Doppler information from observations are represented in nodes, while the spatio-temporal coupling relationship among multi-frame observations is represented in edges. Then the Multi-feature Link Prediction Network (MFLPN) is designed to carry out the multi-frame detection process within observation association graphs. Our contributions are summarized as follows.

- 1) By modeling the multi-frame detection as a link prediction task in graphs, we overcome the performance bottleneck in traditional MFD methods, which arises from model mismatches and insufficient utilization of echo information during the sequential track search and detection. By constructing multi-frame observations as observation association graphs, we perform a link prediction task to directly output target tracks, which enables integrated track search and detection, ensuring effective suppression of false alarms while achieving superior target detection performance.
- 2) By integrating information such as echo structures, Doppler measurements, and spatio-temporal coupling, we specifically design the Multi-feature Link Prediction Network which effectively exploits multi-dimensional features and leverage a unified network cost function to enable the network to perform link prediction tasks with greater accuracy.
- 3) We construct edge features based on coupled position and Doppler measurements. A novel message passing function is designed to integrate edge features while incorporating an attention mechanism. This approach effectively extracts spatio-temporal coupling information among plots, thereby enhancing the network performance.

The rest of this article is organized as follows. Section II briefly describes the MFD problem. Sections III and IV introduce the design of the GLP-MFD and its corresponding computational complexity analysis, respectively. Section V presents numerical results to validate

the performance improvements of the proposed algorithm. Finally, Section VI concludes this article.

II. PROBLEM FORMULATION

Coherent radar systems can improve the target SNR through pulse compression and coherent integration, while obtaining Doppler measurements. After detection with the primary threshold and plot extraction, the k -th observation at frame n can be represented as a vector:

$$\mathbf{z}_{k,n} = (t_{k,n}, r_{k,n}, \theta_{k,n}, v_{k,n}, \mathbf{a}_{k,n})^\top, \quad (1)$$

where $t_{k,n}$ is the time instant when the observation is taken, $r_{k,n}$ is the range measurement, $\theta_{k,n}$ is the azimuth measurement, $v_{k,n}$ is the potentially ambiguous radial velocity, $\mathbf{a}_{k,n}$ is the range-Doppler map and \top denotes the transpose operation. For better readability, we consider a 2-D radar scenario, but the proposed algorithm can be easily extended to 3-D radar scenarios that include elevation information. The relationship between the true target state in Cartesian coordinates $(x_{k,n}, \dot{x}_{k,n}, y_{k,n}, \dot{y}_{k,n})$ and the radar measurements is as follows:

$$\begin{aligned} r_{k,n} &= \sqrt{x_{k,n}^2 + y_{k,n}^2} + w_{k,n}^r \\ \theta_{k,n} &= \arctan \frac{y_{k,n}}{x_{k,n}} + w_{k,n}^\theta \\ v_{k,n} &= \left(\frac{\dot{x}_{k,n} \cdot x_{k,n} + \dot{y}_{k,n} \cdot y_{k,n}}{\sqrt{x_{k,n}^2 + y_{k,n}^2}} + \frac{v_u}{2} \right) \bmod v_u \\ &\quad - \frac{v_u}{2} + w_{k,n}^v, \end{aligned} \quad (2)$$

where v_u denotes the range of the unambiguous radial velocity. $w_{k,n}^r$, $w_{k,n}^\theta$ and $w_{k,n}^v$ represent the noise of range, azimuth and radial velocity measurements, respectively. All three are zero-mean additive Gaussian white noise, with standard deviations proportional to the range, azimuth and velocity resolution, and inversely proportional to the square root of the SNR. Considering range ambiguity can be resolved by using techniques such as frequency stepping or transmitting orthogonal waveforms, we only focus on the potential ambiguity in radial velocity. The observation list corresponds to D_n plots obtained in frame n is defined as follows:

$$\mathbf{Z}_n = (\mathbf{z}_{1,n}, \mathbf{z}_{2,n}, \dots, \mathbf{z}_{D_n,n}). \quad (3)$$

The task of multi-frame target detection is to determine whether a target exists within the multi-frame observations $\{\mathbf{Z}_l\}_{l=n}^{n+L-1}$, where L represents the number of frames processed jointly, also known as the length of processing sliding window. The operating scheme of the proposed GLP-MFD algorithm is depicted in Fig. 1. First, multi-frame observations that exceed the primary threshold γ_1 are roughly associated to construct observation association graphs. Subsequently, MFLPN is employed to complete the integrated track search and track detection process within the observation association graphs, after which the confidence score for each candidate track is

obtained. The candidate track with a confidence score exceeding γ_2 will be declared as the potential track. Finally, confirmed target tracks are output after track pruning, which can be used for subsequent operations such as target tracking. The primary threshold γ_1 determines the optimal detection performance of the proposed scheme. To enhance the detection capability for weak targets, γ_1 is typically set to a relatively low value. Additionally, it is essential to minimize false alarms to prevent imposing an undue computational burden on the system.

III. MULTI-FRAME DETECTION VIA GRAPH NEURAL NETWORK-BASED LINK PREDICTION

The proposed GLP-MFD algorithm first utilizes prior knowledge of target kinematics and employs relaxed constraints tailored to the target to perform a rough association of multi-frame observations that exceed the primary threshold, thereby forming observation association graphs. This approach enables target plots to readily meet the constraints, ensuring successful associations and preventing performance degradation due to association failures. Then, we design MFLPN that integrates track search and track detection. Specifically, the Node Feature Embedding Network (NFEN) is developed to extract plot features such as echo structure and Doppler information by leveraging the strong fitting capabilities of Deep Neural Networks (DNNs) for nonlinear mapping[36],[37]. Subsequently, we design the Graph Attention Network with Spatio-Temporal Coupling Encoded in Edge Features (STEF-GAN) based on GNNs. By incorporating an attention mechanism and constructing edge features during message passing, this network more adequately extracts relational information that embody physical motion patterns among target plots. Finally, we develop an Observation Association Judgment Network (OAJN) to utilize the link prediction concept in order to output potential tracks, which will be declared as confirm tracks after pruning.

By employing the aforementioned data-driven approach to learn the complex nonlinear mapping from multi-frame information to target detection, the method integrates the two sequential steps into one, thereby simplifying the processing logic while reducing loss. Furthermore, it effectively leverages multi-dimensional features on different attributes, such as echo structure and spatio-temporal coupling information, resulting in superior performance in detecting weak targets while effectively suppressing false tracks.

A. Construction of observation association graphs

The target plots exhibit a certain spatio-temporal correlation across frames, allowing for using prior knowledge of target kinematics to roughly associate multi-frame observations that exceed a relative low primary threshold. An undirected graph $\mathcal{G} = (\mathcal{V}, \mathcal{E})$, referred to as the observation association graph is constructed,

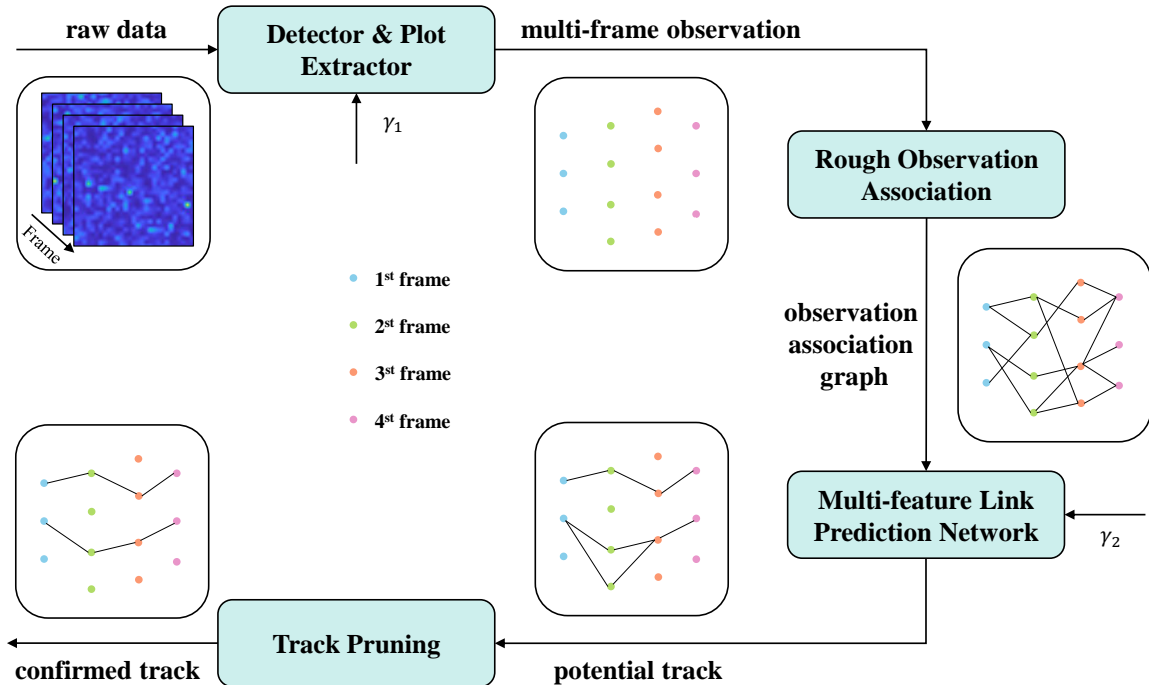


Fig. 1: Operating scheme of GLP-MFD.

where \mathcal{V} denotes the set of nodes representing multi-frame observations and \mathcal{E} signifies the set of edges that connect successfully associated nodes. Correct target tracks exist within the graph, and we aim to accurately finding target tracks while eliminating false tracks. Due to the limited computational power of the system, it is unreasonable to associate all observations across frames and instead, multi-frame observations should be associated based on a certain constraint. To mitigate performance loss due to target missed associations, the selected constraint should be adaptable to targets. Since the velocities of the targets of interest typically have an upper bound, we leverage the velocity limit to ensure successful target association while roughly excluding false observations unlikely to be associated with targets, thereby reducing computational burden. Therefore, observation association graphs are constructed by using the maximum velocity constraint.

For two observations $(t_1, r_1, \theta_1, v_1)$ and $(t_2, r_2, \theta_2, v_2)$ from different frames, where $t_1 < t_2$, the maximum velocity constraint is as follows:

$$\begin{aligned} \|\mathbf{p}_2 - \mathbf{p}_1\| &\leq v_{\max}(t_2 - t_1) \\ \mathbf{p}_1 &= (r_1 \cos \theta_1, r_1 \sin \theta_1) \\ \mathbf{p}_2 &= (r_2 \cos \theta_2, r_2 \sin \theta_2). \end{aligned} \quad (4)$$

where, v_{\max} denotes the maximum velocity of the targets of interest and $\|\cdot\|$ denotes the magnitude.

The observations in multi-frame data $\{\mathbf{Z}_l\}_{l=n}^{n+L-1}$ that satisfy the maximum velocity constraint will be associated. Due to the difficulty in reliably detecting low SNR targets in every frame, and to ensure successful target association and track continuity, we stipulate that observations need to undergo association testing with those in subsequent Q frames. Correspondingly, the maximum

number of consecutive missed detections allowed for a track is set to $Q - 1$. If a track has Q consecutive frames without observations, it is deemed to be of poor quality and should be discarded. A sample of the constructed observation association graph is illustrated in Fig. 2, demonstrating the effective associations among target plots, which helps to avoid missed associations due to model mismatches. Additionally, the number of plots in the confirmed track is set to be at least M . In other words, any path in the graph with M or more nodes is considered as a candidate track. And the link prediction acts on these candidate tracks to eliminate associations containing false alarms while preserving the associations between targets, thereby achieving integrated track search and track detection.

B. Multi-feature Link Prediction Network

Given the challenges in deriving an optimal detector that effectively integrates multi-dimensional information, we address the problem from a data-driven perspective. By cleverly designing networks and the cost function, we achieve a near-optimal fusion detector that comprehensively utilizes diverse information on different attributes. The architecture of MFLPN is illustrated in Fig. 3. After constructing observation association graphs, NFEN first performs feature extraction on the multi-dimensional information of plots. Next, STEF-GAN is employed to extract spatio-temporal coupling features between plots, enhancing the fusion of multi-frame information. Finally, OAJN is utilized to conduct the link prediction task, yielding confidence for edges derive from target associations, and subsequently obtaining the confidence of

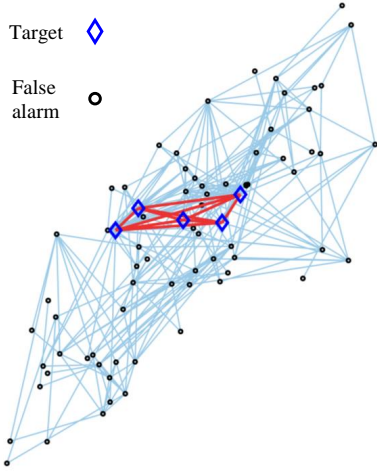


Fig. 2: Schematic of the observation association graph.

candidate tracks originating from targets. Based on the track confidence, the second threshold γ_2 is employed to make detection for candidate tracks, with those exceeding γ_2 regarded as potential target tracks.

1) *NFEN Layer*: Information such as Doppler and echo structure can be obtained in the coherent radar system. By fully integrating these information, the algorithm performance should be enhanced. The plot information we use is as follows:

$$\mathbf{z}_{k,n} = (t_{k,n}, r_{k,n}, \theta_{k,n}, v_{k,n}, d_{k,n}, s_{k,n}, \mathbf{i}_{k,n}, \mathbf{a}_{k,n})^\top, \quad (5)$$

where $d_{k,n}$ represents the Doppler channel in which the observation is detected, $s_{k,n}$ represents SNR, $\mathbf{i}_{k,n}$ represents temporal information, and $\mathbf{a}_{k,n}$ represents the range-Doppler map. The variation of the Doppler channel $d_{k,n}$ where the target plot is located across multiple frames reflects the target kinematic characteristics. For example, when a target moves at a constant speed, its Doppler channel remains stable or varies approximately linearly. The signal-to-noise ratio $s_{k,n}$ not only reflects the strength of the target signal but also indicates the magnitude of measurement errors. Therefore, the information held by SNR is valuable and warrants thorough exploration. The temporal information represents the chronological order of the observations in the track, serving as important temporal scale information. In this paper, the frame n is converted to binary encoding as a temporal feature, denoted as $\mathbf{i}_{k,n}$. As shown in Fig. 4, the signal structures of target observations across multiple frames exhibit a certain similarity, which is an important feature for distinguishing targets and false alarms. After coherent integration, the corresponding range-Doppler maps which contain signal structure information for specific detection units can be obtained. We leverage range-Doppler maps to further extract characteristics of targets in the signal domain, thereby enhancing the separability between targets and false alarms.

The NFEN aims at performing feature extraction on $\mathbf{h}_{k,n} = (d_{k,n}, s_{k,n}, \mathbf{i}_{k,n}, \mathbf{a}_{k,n})^\top$, which in turn makes the

whole network better at fusing multi-dimensional information. It contains three fully connected neural networks and one convolutional neural network. The fully connected layer is usually used for feature enhancement and transformation of dimensions. The convolutional structure not only reduces the number of parameters through parameter sharing, but also improves the learning ability of NFEN for local similarity information, which in turn leads to more effective extracting of plot features.

The transformations from $d_{k,n}, s_{k,n}, \mathbf{i}_{k,n}$ to their feature vectors $\mathbf{f}_{k,n}^{(d)}, \mathbf{f}_{k,n}^{(s)}, \mathbf{f}_{k,n}^{(i)}$ are achieved using fully connected neural networks:

$$\begin{aligned} \mathbf{f}_{k,n}^{(d)} &= \left(D_d^{(N_d)} \circ \dots \circ D_d^{(1)} \right) (d_{k,n}) \\ &= \phi_D \left(\mathbf{W}_d^{(N_d)} \dots \phi_D \left(\mathbf{W}_d^{(1)} d_{k,n} \right) \right) \\ \mathbf{f}_{k,n}^{(s)} &= \left(D_s^{(N_s)} \circ \dots \circ D_s^{(1)} \right) (s_{k,n}) \\ &= \phi_D \left(\mathbf{W}_s^{(N_s)} \dots \phi_D \left(\mathbf{W}_s^{(1)} s_{k,n} \right) \right) \\ \mathbf{f}_{k,n}^{(i)} &= \left(D_i^{(N_i)} \circ \dots \circ D_i^{(1)} \right) (\mathbf{i}_{k,n}) \\ &= \phi_D \left(\mathbf{W}_i^{(N_i)} \dots \phi_D \left(\mathbf{W}_i^{(1)} \mathbf{i}_{k,n} \right) \right), \end{aligned} \quad (6)$$

where D_i denotes the transformations between layers, \circ denotes the composition of functions, N_d, N_s, N_i denote the number of fully connected layers, $\mathbf{W}_d, \mathbf{W}_s, \mathbf{W}_i$ denote the learnable parameter matrixes and ϕ_D denotes the nonlinear activation function in NEFN, which enhances the ability to learn nonlinear mappings. The transformation from $\mathbf{a}_{k,n}$ to its feature vector $\mathbf{f}_{k,n}^{(a)}$ is completed using a convolutional neural network:

$$\begin{aligned} \mathbf{f}_{k,n}^{(a)} &= \left(D_a^{(N_a)} \circ \dots \circ D_a^{(1)} \right) (\mathbf{a}_{k,n}) \\ &= \phi_D \left(\mathbf{W}_a^{(N_a)} * \dots * \phi_D \left(\mathbf{W}_a^{(1)} * \mathbf{a}_{k,n} \right) \right), \end{aligned} \quad (7)$$

where N_a denotes the number of convolutional layers, $*$ denotes the circular convolution operation and \mathbf{W}_a denotes the parameters in the convolution kernels. Finally, the concatenation of $\mathbf{f}_{k,n}^{(d)}, \mathbf{f}_{k,n}^{(s)}, \mathbf{f}_{k,n}^{(i)}, \mathbf{f}_{k,n}^{(a)}$ yields the multi-dimensional fused feature of the plot:

$$\mathbf{f}_{k,n} = \left[\mathbf{f}_{k,n}^{(d)}; \mathbf{f}_{k,n}^{(s)}; \mathbf{f}_{k,n}^{(i)}; \mathbf{f}_{k,n}^{(a)} \right], \quad (8)$$

where the fused feature $\mathbf{f}_{k,n}$ is used as the input node feature of the STEF-GAN layer in observation association graphs. To enhance readability, we reformulate the input node features based on the temporal order of the observations across multiple frames. Specifically, if there are D_l observations in the l -th frame across L frames, $l = 1, 2, \dots, L$, the input node features are rewritten as $\mathbf{x}_1^{(0)}, \mathbf{x}_2^{(0)}, \dots, \mathbf{x}_{\mathcal{L}}^{(0)}$, where $\mathcal{L} = \sum_{l=1}^L D_l$.

2) *STEF-GAN Layer*: Most existing Graph Neural Networks can be abstractly summarized into a universal framework known as Message Passing Neural Networks (MPNNs)[38]. MPNNs focus on a specific message passing mechanism, allowing for the transfer of node information by defining a message passing function, enabling each node to aggregate information from its neighbors and

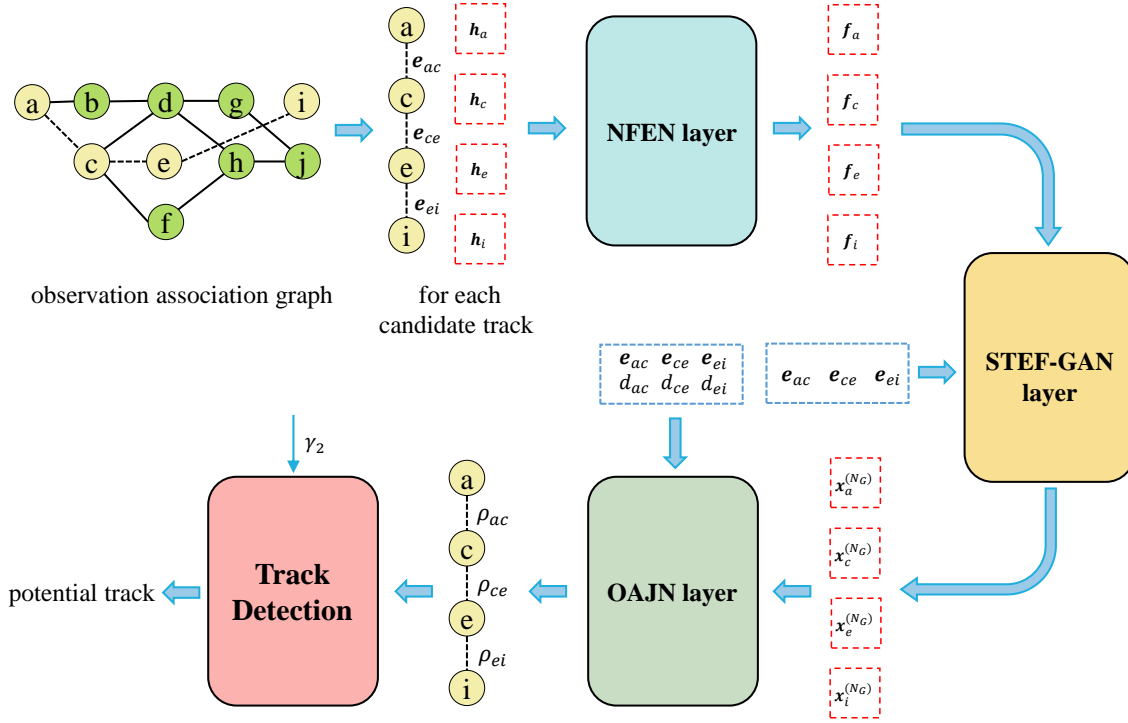


Fig. 3: The architecture of Multi-feature Link Prediction Network.

update its state accordingly. The design of contemporary GNNs mostly adheres to this message passing concept.

The observation association graphs constructed from data received by sensors at different times are distinct, indicating that the problem we address is an inductive task. Introducing an attention mechanism allows the network to focus more on globally relevant information that aids decision-making, enabling efficient resource utilization and enhancing the network's generalization capability, particularly performing well in inductive tasks[39],[40]. Furthermore, incorporating edge features facilitates a more thorough exploitation of the spatio-temporal coupling characteristics among multi-frame observations, thereby improving the network performance. Based on these considerations, the message passing formula of the k -th layer in STEF-GAN is as follows:

$$\begin{aligned}
 \mathbf{x}_i^{(k+1)} &= \phi_G \left(\mathbf{W}_G^{(k)} \mathbf{x}_i^{(k)} \oplus_{j \in \mathcal{N}(i)} \right. \\
 &\quad \left. a_{j,i}^{(k)} \beta_G^{(k)} \left(\mathbf{W}_G^{(k)} \mathbf{x}_j^{(k)} \parallel \mathbf{L}_E^{(k)} e_{j,i} \right) \right) \\
 a_{j,i}^{(k)} &= \frac{M_{j,i}^{(k)}}{\sum_{m \in \mathcal{N}(i)} M_{m,i}^{(k)}} \\
 M_{m,i}^{(k)} &= \exp \left(\text{LeakyRelu} \left(\mathbf{h}_G^{(k)} \left(\mathbf{W}_G^{(k)} \mathbf{x}_i^{(k)} \parallel \right. \right. \right. \\
 &\quad \left. \left. \left. \mathbf{W}_G^{(k)} \mathbf{x}_m^{(k)} \parallel \mathbf{W}_E^{(k)} e_{m,i} \right) \right) \right).
 \end{aligned} \tag{9}$$

$\mathbf{x}_i^{(k)}$ denotes the feature of node i in the k -th layer and the input node feature matrix $\mathbf{x}^{(0)}$ of STEF-GAN is the output fused feature matrix \mathbf{f} of NFEN. $\mathcal{N}(i)$ denotes

the set of neighboring nodes of i and $e_{j,i}$ denotes the feature of the edge between node i and node j . $\mathbf{W}_G^{(k)}$ and $\mathbf{L}_E^{(k)}$ are the learnable matrixes of nodes and edges, respectively. ϕ_G denotes the nonlinear activation function in STEF-GAN such as ReLU, sigmoid and softmax. $\beta_G^{(k)}$ represents a fully connected layer and \parallel is a concatenation operation. \oplus represents an aggregation operation, such as summation, maximization, or averaging, which integrates the information from the neighboring nodes of i into itself. In the attention mechanism, $a_{j,i}^{(k)}$ represents the attention coefficient at the k -th layer, while $\mathbf{h}_G^{(k)}$ represents the learnable parameters and $\mathbf{W}_E^{(k)}$ represents the learnable matrix for edges. Unlike $\mathbf{L}_E^{(k)}$ which focuses on enhancing edge features, $\mathbf{W}_E^{(k)}$ emphasizes learning the impact of edge features within the attention mechanism. Additionally, employing multi-head attention mechanism can enhance the stability of the training process and improve the network accuracy[41],[42]. In this case, the message passing formula is rewritten as follows:

$$\mathbf{x}_i^{(k+1)} = \parallel_{h=1}^H \mathbf{x}_i^{(k+1,h)}. \tag{10}$$

H is the number of heads with $\mathbf{x}_i^{(k+1,h)}$ representing the aggregated feature of node i in the h -th head, which independently executes the transformation shown in (9). It is precisely that the message passing mechanism which enables STEF-GAN to integrate multi-frame spatial-temporal information and reveal the relationship between observations, thereby enhancing the separability of targets and false alarms.

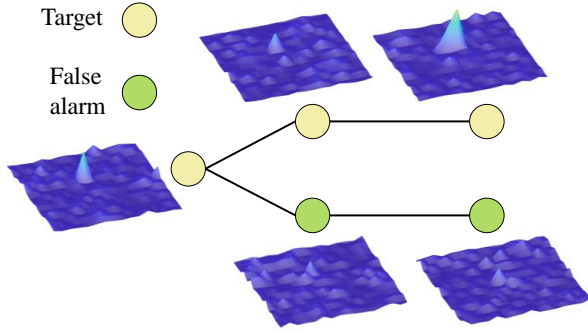


Fig. 4: Illustration of the signal structural difference between targets and false alarms.

The time, range, azimuth and radial velocity measurements of target plots exhibit a certain coupling relationship across frames, reflecting the target physical kinematics. However, this coupling relationship is often complex. Directly using $t_{k,n}, r_{k,n}, \theta_{k,n}, v_{k,n}$ as the node feature input to the network will increase both the training difficulty and computational burden. To address this issue, we pre-construct the mapping relationships of observation measurements across multiple frames according to the target kinematics and treat the relationships as edge features. This method effectively extracts the spatio-temporal coupling features among multi-frame observations while ensuring computational efficiency and maintaining good performance.

In practice, target motion is typically based on a certain physical mechanism. For example, considering a target moving at a constant speed, it is possible to use the position measurements in two frames to estimate the target velocity. By projecting this velocity onto the sensor line-of-sight directions in each frame, the estimation of target radial velocities in both frames can be derived. If there are no measurement errors, the estimated velocities should be equal to the velocity measurements. Considering the presence of errors, there will be a certain deviation between the estimations and the measurements, which can be used to determine whether two observations correspond to the same target. Therefore we incorporate the deviation as the edge feature in STEF-GAN to learn the confidence that two observations originate from the same target.

For two observations $(t_1, r_1, \theta_1, v_1)$ and $(t_2, r_2, \theta_2, v_2)$ from different frames, where $t_1 < t_2$, the observed radial velocities can be expressed as follows while taking into account the potential radial velocity ambiguities.

$$\begin{aligned} v_1 + m_1 v_u, \quad m_1 \in \mathbb{Z} \\ v_2 + m_2 v_u, \quad m_2 \in \mathbb{Z}, \end{aligned} \quad (11)$$

where v_u denotes the range of the unambiguous radial velocity while m_1 and m_2 denote the ambiguous numbers. The target moving velocity can be estimated based on the position measurements, and by projecting this velocity

along the sensor line-of-sight, the target estimated radial velocities can be obtained:

$$\begin{aligned} \hat{v}_1 &= \frac{r_2 \cos(\theta_2 - \theta_1) - r_1}{t_2 - t_1} \\ \hat{v}_2 &= \frac{r_2 - r_1 \cos(\theta_2 - \theta_1)}{t_2 - t_1} \end{aligned} \quad (12)$$

For the same target, there is a certain deviation between the estimated radial velocities and the observed radial velocities. We incorporate the deviation as a feature input to the network[33]:

$$\begin{aligned} F_{MC,1} &= |v_1 + m_1 v_u - \hat{v}_1| \\ F_{MC,2} &= |v_2 + m_2 v_u - \hat{v}_2| \\ m_1 &= \arg \min_{m \in \mathbb{Z}} |v_1 + m_1 v_u - \hat{v}_1| \\ m_2 &= \arg \min_{m \in \mathbb{Z}} |v_2 + m_2 v_u - \hat{v}_2|. \end{aligned} \quad (13)$$

Since $F_{MC,1}$ and $F_{MC,2}$ are features derived from the information of two nodes, they can serve as edge features in observation association graphs, denoted as $e_{1,2} = [F_{MC,1}, F_{MC,2}]$.

In summary, after obtaining the input features for nodes and edges in observation association graphs, the STEF-GAN leverages multi-layer message passing to extract information from multiple frames:

$$\mathbf{X}^{(N_G)} = \left(G^{(N_G)} \circ \dots \circ G^{(2)} \circ G^{(1)} \right) (\mathbf{x}^{(0)}, e), \quad (14)$$

where G denotes the transformations between layers and N_G is the number of layers. $\mathbf{x}^{(0)}$ represents the node feature matrix input to STEF-GAN, which is also the plot fused feature matrix \mathbf{f} output from NEFN and e represents the edge feature matrix.

3) *OAJN Layer*: After thoroughly extracting multi-dimensional features of plots and spatio-temporal coupling features among multi-frame plots, we employ OAJN to achieve intelligent and integrated track search and track detection process within observation association graphs. Compared to traditional methods that utilize energy accumulation compared with a given threshold for track detection[18], this approach excels in learning the mapping from measurement information to whether plot associations stem from the target, thus providing a better assessment of the track quality. The proposed method first accomplishes a link prediction task, classifying edges to obtain the confidence that the plot associations originate from the target. Subsequently, it determines the confidence that the candidate tracks are derived from the target and conducts track detection based on a second detection threshold γ_2 .

Considering that $e_{j,i} = [F_{MC,j}, F_{MC,i}]$ directly reflects the coupling relationship between position and Doppler measurements, we reintegrate edge features into OAJN for more effective utilization. Additionally, the difference in Doppler channels of the target is an important feature for target motion characteristics. For instance, the difference in Doppler channels of a target moving at a constant speed across different frames is typically small.

As a consequence, we also incorporate the Doppler channel difference $d_{j,i} = |d_j - d_i|$ between node i and node j into OAJN to enhance the learning of link prediction. To facilitate the subsequent distinguishing between target tracks and false tracks based on the second threshold, we select the softmax function as the nonlinear activation when decoding. In the observation association graph, edges are categorized into three types: the edge between false alarms, the edge between a false alarm and a target, and the edge between targets. Their corresponding ground truths are denoted as $y_{j,i}^{(1)}, y_{j,i}^{(2)}, y_{j,i}^{(3)}$. For any two connected nodes i and j , the classification of their edge is expressed as follows:

$$\begin{aligned} \hat{y}_{j,i} &= \left[\hat{y}_{j,i}^{(1)}, \hat{y}_{j,i}^{(2)}, \hat{y}_{j,i}^{(3)} \right] \\ &= \text{softmax} \left(\mathbf{W}_J^{(N_J)} \dots \phi_J \left(\mathbf{W}_J^{(1)} \mathbf{F}_{j,i} \right) \right) \quad (15) \\ \mathbf{F}_{j,i} &= \left[\mathbf{x}_i^{(N_G)}; \mathbf{x}_j^{(N_G)}; \mathbf{e}_{j,i}; d_{j,i} \right], \end{aligned}$$

where $\hat{y}_{j,i}^{(c)}, c = 1, 2, 3$ represents the classification score for edges, indicating the confidence that the edges originate from target associations. $\mathbf{x}_j^{(N_G)}$ and $\mathbf{x}_i^{(N_G)}$ are the output node features of STEF-GAN, while $\mathbf{F}_{j,i}$ is the concatenated feature. \mathbf{W}_J denotes the learnable parameter matrix in OAJN and ϕ_J is the nonlinear activation function. The categorical cross-entropy loss function is employed in this work, which not only alleviates the gradient vanishing problem caused by deep networks but is also equivalent to obtaining a nonlinear mapping from multi-dimensional information in raw data to target detection through maximum likelihood estimation[43]. The categorical cross-entropy loss function used for integrated training is formulated as follows:

$$\mathcal{J}(\theta) = -\frac{1}{N_T} \sum_{n=1}^{N_T} \frac{1}{E_n} \sum_{(j,i) \in \mathcal{E}_n} \sum_{c=1}^3 y_{j,i}^{(c)} \log \hat{y}_{j,i}^{(c)}, \quad (16)$$

where N_T represents the number of graphs in the training set, E_n denotes the number of edges in the n -th graph and \mathcal{E}_n refers to the edge set of the n -th graph.

The confidence S that a candidate track originates from a target is defined as follows:

$$\begin{aligned} S &= \frac{1}{N_E} \sum_{e=1}^{N_E} s_e + \lambda N_V \quad (17) \\ s_e &= \alpha_1 \cdot \hat{y}_e^{(1)} + \alpha_2 \cdot \hat{y}_e^{(2)} + \alpha_3 \cdot \hat{y}_e^{(3)}, \end{aligned}$$

where N_E represents the edge number of the track, N_V represents the track length, $\hat{y}_e^{(c)}, c = 1, 2, 3$ represents the classification score of the e -th edge, α_c and λ are both hyperparameters. For the configuration of hyperparameters, we offers some empirical recommendations. For a target track, the most desirable edges are those between targets, while the least desirable are those between false alarms. Therefore, the weight for the classification score of edges between targets can be set to $\alpha_3 = 1$, while the weight for edges between false alarms can be set to $\alpha_1 = 0$. As to the weight for edges between targets and false alarms, it can be set to a small positive value, such as $\alpha_2 = 0.2$.

On one hand, we aim to preserve as many edges between targets as possible, while also striving to suppress edges between targets and false alarms. Thus, the weight should not be too large. On the other hand, to differentiate from edges between false alarms, and considering the presence of target plots, the weight should preferably be greater than α_1 . Additionally, without affecting subsequent target tracking, associations between targets and false alarms can help to improve track continuity. For example, in scenarios where a weak target is not detected in the current frame, if an association occurs between the historical target track and a false alarm without negatively impacting subsequent target tracking, it can actually improve track continuity.

The weight λ of track length should be balanced with the weights of edges. From one perspective, it should not be set too high, as this may place excessive emphasis on track length, leading to an increase in false alarms within the track. From another perspective, while ensuring that the confidence score for edges originating from target associations is high, longer tracks should be chosen to enhance track continuity. After obtaining the track confidence, a second detection threshold γ_2 is applied for track detection. Tracks that exceed γ_2 are classified as potential target tracks. Finally, following track pruning, the confirmed tracks are generated and output.

IV. COMPUTATIONAL COMPLEXITY ANALYSIS

The computational complexity of the proposed GLP-MFD algorithm primarily consists of two components: the construction of the observation association graph and the Multi-feature Link Prediction Network, which includes the NFEN layer, the STEF-GAN layer, and the OAJN layer. The complexity of constructing the observation association graph is the function of the observations per frame and the number of frames to be processed. Due to the challenges in detecting low SNR targets, it is often difficult to guarantee detection in every frame. Therefore, each observation needs to attempt associations with those in the subsequent Q frames. When forming graphs from L consecutive frames, for the observations in the l -th frame, the maximum velocity constraint is applied for association testing with observations in the set $\{l+1, \dots, \min\{l+Q, L\}\}$. Given that targets are typically sparse in radar observation space, we explore the computational complexity under the case where only false alarms are present in each frame. For a radar system with N_r range cells, N_θ beam positions and N_D Doppler channels, when the primary detection threshold γ_1 is set corresponding to the initial false alarm probability $P_{fa,1}$, the average number of required operations N_{GC} for graph construction is as follows[22]:

$$N_{GC} = Q \left(L - \frac{Q}{2} - \frac{1}{2} \right) (N_r N_\theta N_D P_{fa,1})^2. \quad (18)$$

Let N_{fa} represents the expectation of the false alarm number per frame, then we get $N_{fa} = N_r N_\theta N_D P_{fa,1}$.

Consequently, the average computational complexity for graph construction can be simplified to $O(LQN_{fa}^2)$.

The operations involved in the NFEN layer primarily consist of matrix multiplication and element-wise operations, with its computational complexity being a function of the number of parameters. NFEN is divided into two main categories: the convolutional network and the fully connected networks. The number of convolutional layers is denoted as N_a . I_0 and I_{N_a} denote the numbers of input and output channels respectively while I_p ($p = 1, 2, \dots, N_a - 1$) denotes the channels from intermediate convolutional operations. M_p ($p = 1, 2, \dots, N_a$) is the size of the convolutional kernel for each layer and the bias term is set to 1. The total number of parameters for the convolutional network is as follows:

$$N_{t,a} = \sum_{p=0}^{N_a-1} (I_p M_{p+1} + 1) I_{p+1}. \quad (19)$$

Specifically, the numbers of input and output channels are often set to 1.

To simplify the analysis, we assume that the numbers of hidden neurons in three fully connected networks are all set to N_h . Let N_d, N_s, N_i denote the number of layers for $d_{k,n}, s_{k,n}, i_{k,n}$, respectively. The total number of parameters for each of the three fully connected networks can be expressed as follows:

$$\begin{aligned} N_{t,d} &= 2N_h + (N_d - 2)(N_h + 1)N_h + (N_h + 1)N_h \\ N_{t,s} &= 2N_h + (N_s - 2)(N_h + 1)N_h + (N_h + 1)N_h \\ N_{t,i} &= 5N_h + (N_i - 2)(N_h + 1)N_h + (N_h + 1)N_h, \end{aligned} \quad (20)$$

where each term in the formula corresponds to the parameters of the input layer, hidden layers, and the output layer, respectively. The coefficient of N_h in the first term denote the input feature dimension plus a bias which is set to 1. Therefore, the total parameters in NFEN is:

$$N_{t,NEFN} = N_{t,d} + N_{t,s} + N_{t,i} + N_{t,a}. \quad (21)$$

For the STEF-GAN layer, the parameter number of $\mathbf{L}_E^{(k)}$ in all N_G layers is $2N_{LE}$, where 2 is the feature dimension of $e_{j,i}$ and N_{LE} is the dimension of the enhanced edge feature. The parameter number of $\mathbf{W}_G^{(k)}$ is $N_{x_k}N_{x_{k+1}}$, where N_{x_k} represents the feature dimension of nodes in the k -th layer. β_G is a fully connected layer with $(N_{LE} + N_{x_{k+1}})N_{x_{k+1}}$ parameters. The parameter number of $\mathbf{W}_E^{(k)}$ in all N_G layers is $2N_{WE}$, where N_{WE} is the dimension of the output edge feature in the attention mechanism while $\mathbf{h}_G^{(k)}$ has $(N_{WE} + 2N_{x_{k+1}})$ parameters. Therefore, the total number of parameters in STEF-GAN is as follows:

$$N_{t,STEF} = \sum_{k=0}^{N_G-1} [2N_{LE} + N_{x_k}N_{x_{k+1}} + 3N_{WE} + (N_{LE} + N_{x_{k+1}})N_{x_{k+1}} + 2N_{x_{k+1}}] \quad (22)$$

As to the OAJN layers, let N_m and N_J denote the number of hidden neurons and the number of layers with

the bias term set to 1, respectively. The total number of parameters in OAJN according to (15) is as follows:

$$\begin{aligned} N_{t,OAJN} &= (2N_{x_{NG}} + 2 + 1 + 1)N_m \\ &+ (N_J - 2)(N_m + 1)N_m + 3(N_m + 1). \end{aligned} \quad (23)$$

In summary, when performing integrated track search and track detection in an observation association graph, the computational complexity of MFLPN can be expressed as follows:

$$\begin{aligned} O &(N_a M_{\max} I_{\max}^2 + (N_d + N_s + N_i)N_h^2 \\ &+ N_G N_{x,\max}^2 + N_J N_m^2), \end{aligned} \quad (24)$$

where M_{\max} and I_{\max} represent the maximum kernel size and the maximum number of channels in NEFN, respectively. And $N_{x,\max}$ represents the maximum feature dimension of nodes in STEF-GAN.

In practical engineering applications, the sensor observation space can typically be divided into N_k subareas. Tracks are searched and detected independently within each subarea to reduce the computational burden on the system. Thereby the computational complexity of the graph construction decrease to $O(LQN_{fa}^2/N_k)$. Additionally, parallelizing the initialization of tracks should enhance computational performance. The number of parameters in the network directly determines its computational complexity, allowing for optimization such as pruning the parameters that have minimal impact on the network. Moreover, GPU parallel processing can be utilized for operations like matrix multiplication to further improve computational efficiency.

V. SIMULATION RESULTS

To show the performance improvement in multi-frame detection achieved through the proposed GLP-MFD, we conduct simulation experiments in a 2-D scenario, but the proposed algorithm can be easily extended to 3-D scenarios. The radar system we simulate is based on the L-band carrier frequency with 2° azimuth resolution (3dB antenna), 100m range resolution and 32 pulses transmitted at each beam position. As previously mentioned, the primary threshold γ_1 determines the optimal detection performance that the proposed method can achieve. Therefore, to ensure effective detection performance for weak targets while avoiding excessive false alarms that will impose a computational burden on the system, we set γ_1 corresponding to an initial false alarm probability $P_{fa,1} = 10^{-3}$. Additionally, it is assumed that false alarms originate from receiver internal noise, which is generally valid for long-range target detection.

When processing multi-frame data using neural networks, the relationship among the second threshold γ_2 , the final false alarm probability and the detection probability is complex. Consequently, the false alarm probability and detection probability of the proposed algorithm are calculated using Monte Carlo simulations in this work. Since GLP-MFD transforms plot-level detection into track-level detection, the final false alarm probability $P_{fa,2}$ based on

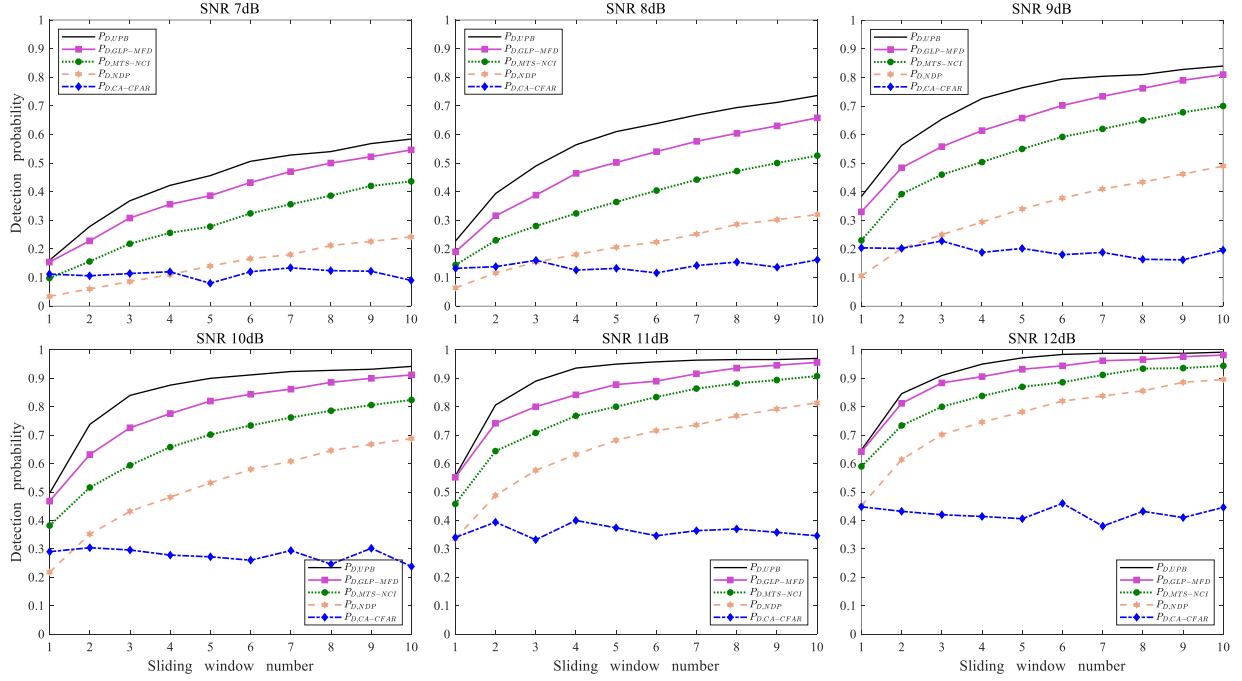


Fig. 5: The detection probability versus the sliding window number.

γ_2 is defined as the total number of false tracks divided by the total number of detection units. The detection probability is defined as the total number of correctly detected target tracks divided by the total number of targets appearance in the Monte Carlo experiments.

A. The definition of correct target detection

The proposed GLP-MFD enables direct output of target tracks through the link prediction task in observation association graphs. To evaluate the performance of GLP-MFD, it is necessary to define whether the output track correspond to a correct target track. Due to measurement noise and the dense false alarm environment, it is possible for a false alarm to exhibit a quality superior to that of a true target measurement, which may lead to the inclusion of false alarms in the initiated target track. However, if the existence of false alarms does not affect subsequent target tracking, the initiated target track can still be considered as a correct target track.

In light of the points mentioned above, we employ the Optimal Subpattern Assignment (OSPA) distance to determine whether the output target track has been correctly detected[44]. The OSPA distance is a metric used in target tracking tasks to measure the difference between the set of estimated target states and true target states at a given time by defining a distance measure in the state space. Given that the OSPA distance is essentially a metric for measuring discrepancy between sets, in the context of this work, we use it to quantify the difference between the smoothed confirmed target tracks output from MFLPN and the tracks with correct target states,

thereby determining whether the output target tracks are indeed correct. Techniques such as linear regression, quadratic regression, and Kalman filtering can be utilized as smoothing algorithms. The formula for the OSPA distance in the context of our work is as follows:

$$d_\xi^{(\eta)}(\mathbf{X}, \hat{\mathbf{X}}) = \left(\frac{1}{N_{\hat{\mathbf{X}}}} \min_{\pi \in \Pi_{N_{\hat{\mathbf{X}}}}} \sum_{i=1}^{N_{\mathbf{X}}} d^{(\eta)}(\mathbf{x}_i, \hat{\mathbf{x}}_{\pi(i)})^\xi + \frac{\eta^\xi}{N_{\hat{\mathbf{X}}}} (N_{\hat{\mathbf{X}}} - N_{\mathbf{X}}) \right)^{1/\xi}, N_{\mathbf{X}} \leq N_{\hat{\mathbf{X}}} \quad (25)$$

$$d_\xi^{(\eta)}(\mathbf{X}, \hat{\mathbf{X}}) = d_\xi^{(\eta)}(\hat{\mathbf{X}}, \mathbf{X}), N_{\mathbf{X}} > N_{\hat{\mathbf{X}}}$$

$$d^{(\eta)}(\mathbf{x}_i, \hat{\mathbf{x}}_{\pi(i)}) = \min(\eta, d(\mathbf{x}_i, \hat{\mathbf{x}}_{\pi(i)})),$$

where $\hat{\mathbf{X}} = (\hat{\mathbf{x}}_1, \hat{\mathbf{x}}_2, \dots, \hat{\mathbf{x}}_{N_{\hat{\mathbf{X}}}})$ represents the set of smoothed confirmed target tracks output from MFLPN, $\mathbf{X} = (\mathbf{x}_1, \mathbf{x}_2, \dots, \mathbf{x}_{N_{\mathbf{X}}})$ represents the set of tracks with correct target states, $\hat{\mathbf{x}}_i$ and \mathbf{x}_i represent the plot position in tracks, $N_{\hat{\mathbf{X}}}$ and $N_{\mathbf{X}}$ represent the total plot number of tracks, $d(\mathbf{x}_i, \hat{\mathbf{x}}_{\pi(i)})$ represents the Euclidean distance between \mathbf{x}_i and $\hat{\mathbf{x}}_{\pi(i)}$, $\Pi_{N_{\hat{\mathbf{X}}}}$ represents the set of permutations on $\{1, 2, \dots, N_{\hat{\mathbf{X}}}\}$, ξ represents the order parameter and η represents the cutoff parameter.

ξ affects the deviation between the estimation and the true value. As ξ increases, the weight of $d_\xi^{(\eta)}(\mathbf{X}, \hat{\mathbf{X}})$ relative to the position error enhances. η influences the discrepancy in the number of plots between smoothed tracks and correct tracks. As η increases, the weight of $d_\xi^{(\eta)}(\mathbf{X}, \hat{\mathbf{X}})$ with respect to the mismatch in the number of plots enhances. In the context of our work, we focus on the impact of false alarms on the quality of target tracks, with greater emphasis placed on position errors. Considering practicality and the smoothness of distance curves, we

set $\xi = 2$. Additionally, the value of η should be relatively small. After evaluating the position measurement errors in terms of the variance of measurement noise, the value of η determined based on the position measurement errors can be regarded as a small value[45]. Given that the range of $d_{\xi}^{(\eta)}(\mathbf{X}, \hat{\mathbf{X}})$ is $[0, \eta]$, when the OSPA distance between smoothed tracks and tracks with correct target states meets the following condition:

$$d_{\xi}^{(\eta)}(\mathbf{X}, \hat{\mathbf{X}}) < \kappa\eta, \quad (26)$$

the confirmed tracks output from the network can be considered as correct target tracks. In (26), the configuration of κ needs to ensure that the trajectories of perceived correct target tracks output from the network are approximately consistent with the tracks with correct target states, without negatively impacting subsequent tracking. This can be achieved by performing Monte Carlo experiments to statistically evaluate the OSPA distance between smoothed tracks consisting entirely of target measurements and the tracks with correct target states, using this evaluation as a reference for setting κ .

B. The detection performance analysis

To demonstrate the superiority of the proposed GLP-MFD algorithm, a comparison is conducted with the traditional search-before-detect MFD method (NDP) and the MFD method that combines model-driven track initiation with non-coherent integration (MTS-NCI). The NDP method constructs potential tracks using kinematic constraints derived from target position measurements and makes track detection through non-coherent integration of track energy followed by comparison with a second threshold. The MTS-NCI method leverages Doppler information, creating kinematic constraints based on the coupling relationship between position and Doppler measurements to obtain potential tracks. By incorporating Doppler information, the separability between targets and false alarms is enhanced. Subsequently, the method accumulates track energy incoherently and makes track detection based on a second threshold. It is important to note that the NDP method does not utilize Doppler information. In the experimental scenario set for this work, if the NDP method uses the primary threshold corresponding to the initial false alarm probability $P_{fa,1} = 10^{-3}$, it will lead to a combinatorial explosion, resulting in an unmanageable computational load. Additionally, due to its poor separability between targets and false alarms, an excessive number of false alarms will adversely impact correct associations of target measurements, degrading the performance of target detection. Therefore, for the NDP method, we employ the primary threshold corresponding to the initial false alarm probability $P_{fa,1,NDP} = 10^{-4}$. The proposed GLP-MFD method and the MTS-NCI method both utilize the primary threshold corresponding to $P_{fa,1} = 10^{-3}$. To ensure a fair comparison, all methods guarantee that the final false alarm probability $P_{fa,2}$ have to be 10^{-6} after processing multi-frame data.

Under the same SNR conditions, the relationship between target detection probabilities and sliding window numbers for aforementioned methods is shown in Fig. 5. $P_{D,CA-CFAR}$ represents the target detection probability in a single frame using the cell-averaging constant false alarm rate (CA-CFAR) algorithm under a false alarm probability of 10^{-6} . $P_{D,UPB}$ denotes the upper limit of detection performance, defined as the probability that a candidate track exists where all plots are target observations across multiple frames. It can be observed from Fig. 5 that as the sliding window number increases, the detection probability of multi-frame detection methods gradually improves. In most cases, multi-frame detection methods achieve better performance compared to CA-CFAR. However, the detection performance of NDP is mostly lower than that of CA-CFAR when the number of sliding windows is small. On one hand, the NDP method does not utilize Doppler information, resulting in poor distinction between targets and false alarms, and the exclusion of false tracks mainly relies on energy accumulation. On the other hand, the primary threshold is set corresponding to $P_{fa,1,NDP} = 10^{-4}$, which restricts the upper limit of detection performance. In contrast, the MTS-NCI method, which incorporates Doppler information, demonstrates better separability between targets and false alarms, outperforming NDP. However, weak targets can diminish the separability and setting $P_{fa,1} = 10^{-3}$ leads to a large number of false alarms. Consequently, when the SNR is 7 dB, the detection performance with a single sliding window is slightly lower than that of CA-CFAR. Whereas, under high SNR conditions, its performance consistently surpasses CA-CFAR.

The proposed GLP-MFD algorithm integrates multi-dimensional information of target observations and spatio-temporal coupling information across multiple frames, approaching a near-optimal detector for fusing features on different attributes and achieving the highest detection performance. Moreover, its superiority becomes more apparent at low SNR compared with NDP and MTS-NCI. It is important to note that in Monte Carlo experiments, situations may arise where a target is not detected by $P_{D,UPB}$, yet the proposed algorithm concludes that the target has been correctly detected. This is because GLP-MFD defines correct detection based on the OSPA distance, which can occasionally obtain the output track where false alarms are present and the number of target plots is less than M . According to the definition of $P_{D,UPB}$, this do not count as a correct detection. However, the compliance of the condition shown in (26) indicates that the false alarms in the track do not affect subsequent target tracking, leading the consideration of correct detection. In practical engineering applications, such high-quality false alarms can also be advantageous for target track initiation.

To completely show the experimental scenario and the overall performance of GLP-MFD, the processing results for one exemplar run are shown in Fig. 6. The observation area of interest is from 100km to 300km and

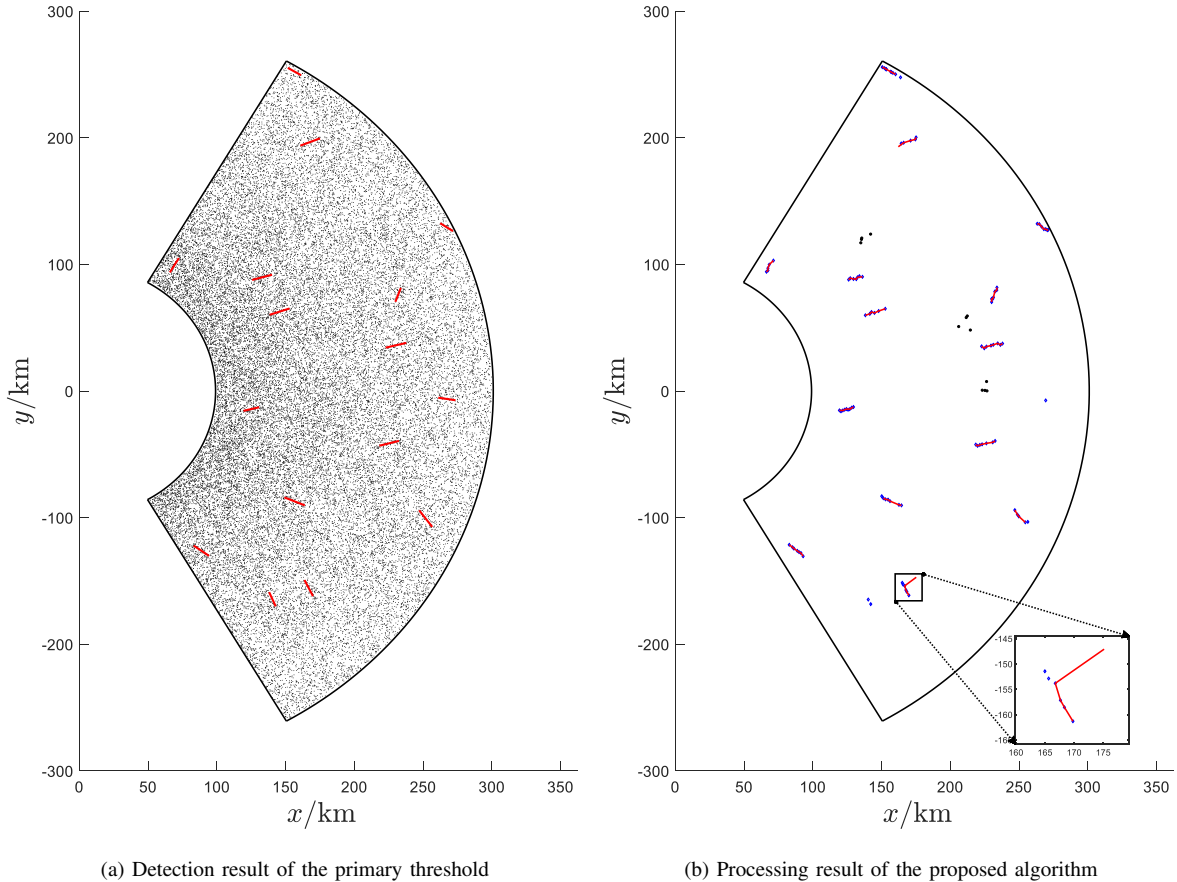


Fig. 6: Results for one exemplar run

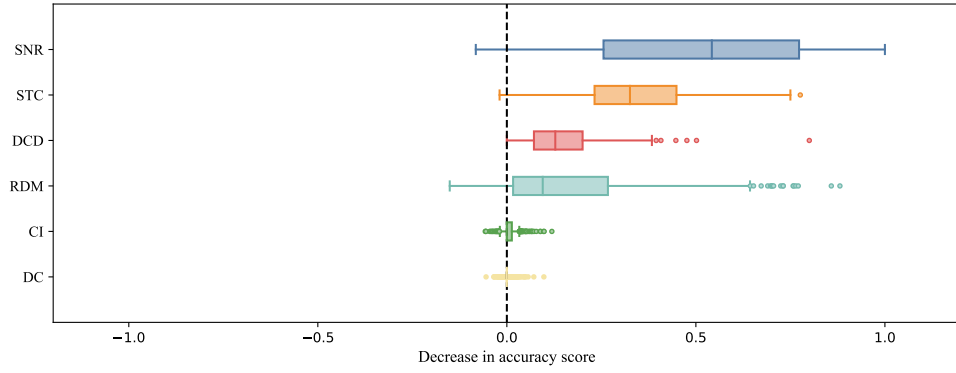
from -60° to 60° containing a total of 16 targets. The detection result corresponding to the primary threshold is shown in 6a, with red solid lines indicating the tracks with correct target states. The processing results of the proposed GLP-MFD is displayed in 6b, where the red solid lines represent the target tracks output from the network, black solid points indicate the false tracks, and blue squares denote the position measurements of targets.

In the processing result, 3 false tracks and 14 target tracks are initiated, while two target tracks are not detected. The retention of false tracks may be due to their alignment with the multi-frame correlation characteristics of targets. However, they can be further eliminated through false track discrimination methods. Among 14 initiated target tracks, 13 are identified as correct target tracks. The enlarged track in the figure has a large OSPA distance from the true target track due to the presence of false alarms, which affects the target track direction and may impact subsequent tracking. Therefore, it cannot be considered correctly detected. Nevertheless, these erroneous target tracks do not impose excessive negative effects. Over continuous multi-frame processing, these incorrect initiations will gradually be filtered out, while the correct target plots within the erroneous tracks will remain and appear in the newly initiated correct tracks.

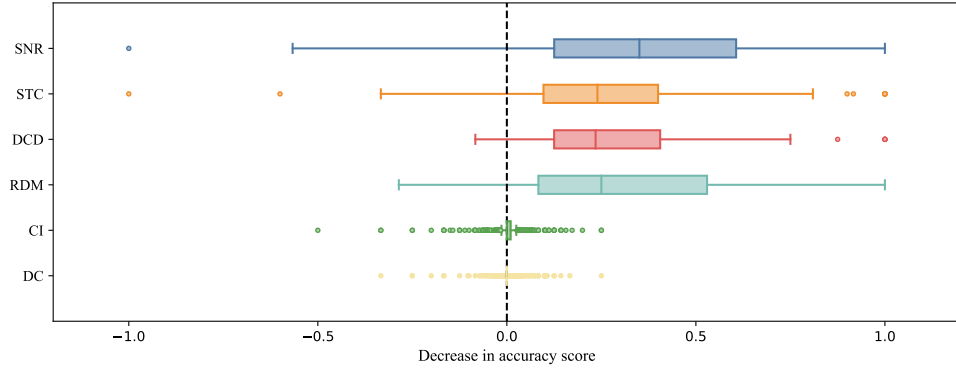
In summary, the proposed GLP-MFD algorithm demonstrates strong detection performance for weak targets and can accurately detect target tracks while effectively suppressing false tracks.

C. Interpretable analysis

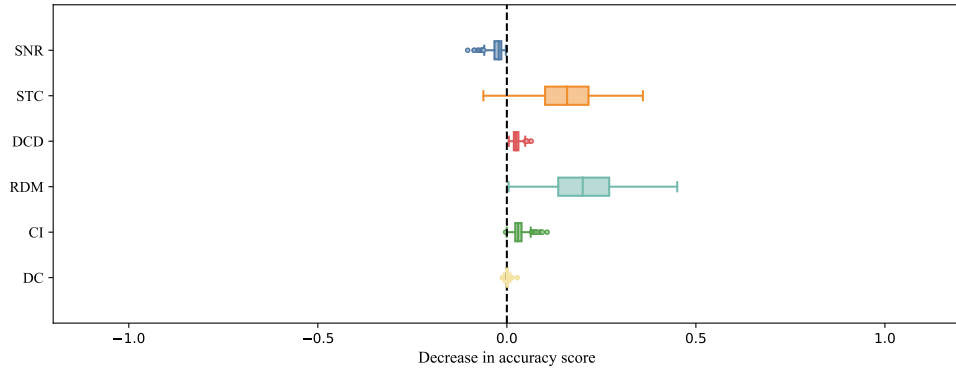
To explore how MFLPN performs integrated track search and track detection based on input features, we analyze the importance of each input feature on the network output. The input features include signal-to-noise ratio (SNR), Doppler channel (DC), chronological information (CI), range-Doppler map (RDM), spatio-temporal coupling (STC) and the differences in Doppler channels (DCD). To analyze the contribution of these features to the network, techniques such as feature occlusion and feature permutation can be employed to eliminate the dependency between samples and their corresponding features. And the decline in network performance can be observed to confirm the importance of each feature[46],[47],[48]. The core task of this work is a link prediction task, which determines whether the associations between measurements originate from targets. To clarify the network decision criteria under different conditions, we use the extent of accuracy decline in link predictions caused by eliminating



(a) Boxplot of feature importance during target association decision at high SNR.



(b) Boxplot of feature importance during target association decision at low SNR.



(c) Boxplot of feature importance during false alarm association decision.

Fig. 7: Boxplots of feature importance during various association decisions.

sample-feature dependencies as a reference metric. The box plots are used to explain the feature importance for the network[49]. The results of association decision in high SNR targets, low SNR targets, and false alarms are shown in Fig. 7.

The results indicate that for high SNR targets, SNR is the most significant feature influencing performance. This is because a higher SNR enhances the separability between targets and false alarms, making it a key characteristic for distinguishing them. The next important features are the spatio-temporal coupling and the dif-

ferences in Doppler channels. Effectively utilizing these features can enhance the accuracy of track initiation for targets with complex physical kinematics. For low SNR targets, although SNR remains the most influential feature, its impact reduces compared to high SNR targets. To compensate, the network increasingly relies on the range-Doppler map, which reflects not only the intensity of echo signals but also the distribution of target echo energy across the range and Doppler dimensions. This structural information facilitates deeper feature extraction by the network. Furthermore, since the network accuracy

in making association decisions for low SNR targets is lower than that for high SNR targets, the range of outliers tends to be larger. In the case of associations between false alarms, the information extracted from SNR of noise measurements is limited, prompting the network to rely more on the range-Doppler map, which contains rich structural information. Additionally, due to the randomness in the distribution of false alarms, the contribution of the differences in Doppler channels decreases, while the spatio-temporal coupling feature becomes critical for the network decision-making. Specifically, if the deviation in the coupling between measured Doppler and position information is small, the association is more likely to stem from a target. Conversely, it is more likely to originate from false alarms.

Thus, through extensive data training, the proposed MFLPN can automatically adjust its association criteria based on data features under different conditions, thereby adaptively selecting corresponding features to make association decisions for observations from various sources. Compared to traditional model-driven methods, the proposed method effectively integrates multi-dimensional information on different attributes to achieve near-optimal unified track search and track detection in multiple frames.

VI. SUMMARY

To address the challenges in traditional single-frame detection methods, which struggle to balance detection performance and system processing burden in weak target detection scenarios, and to overcome the limitations of traditional multi-frame detection methods, where sequential track search and detection are hindered by model mismatches and insufficient utilization of echo information, we propose a multi-frame detection algorithm via graph neural network-based link prediction. The proposed algorithm constructs observation association graphs through a relative low primary threshold, leveraging graph neural networks to fully integrate various information, such as Doppler information, echo structures, and spatio-temporal coupling of multi-frame observations, to complete track search and track detection in a unified manner.

Experiments show that, compared to traditional single-frame and multi-frame detection methods, the proposed algorithm effectively suppresses false tracks while enhancing target detection performance. Moreover, the interpretable analysis reveals that the designed network effectively integrates the input features, enabling precise differentiation of associations between targets and false alarms. However, the multi-frame detection process of the proposed algorithm still involves relatively high computational load. Even though the low threshold eliminates observations unlikely from targets compared to raw data and the integration process follows a relatively straightforward logic, the computational burden during multi-frame joint processing remains substantial. Future work

may consider further enhancing computational efficiency without compromising weak target detection performance.

REFERENCES

- [1] M.A. Richards *Fundamentals of Radar Signal Processing*, 2nd ed. New York, NY, USA: McGraw-Hill, 2014, pp. 406–409.
- [2] *Radar Handbook*, 3rd ed. McGraw-Hill, New York, NY, USA, 2008.
- [3] R. Guo, Y. Yuan, and T. Quan Adaptive modified hough transform track initiator for HFSWR tracking of fast and small targets *J. Syst. Eng. Electron.*, vol. 16, no. 2, pp. 316–320, Jun. 2005.
- [4] A. Farina and F. A. Studer *Radar data processing*. Hoboken, NJ, USA: Wiley, 1985.
- [5] P. Wei, J. Zeidler and W. Ku Analysis of multiframe target detection using pixel statistics *IEEE Trans. Aerosp. Electron. Syst.*, vol. 31, no. 1, pp. 238–247, Jan. 1995, doi: [10.1109/7.366306](https://doi.org/10.1109/7.366306).
- [6] S. J. Davey, M. G. Rutten and B. Cheung A comparison of detection performance for several Track-Before-Detect algorithms In *Proc. Int. Conf. Inf. Fusion*, Cologne, Germany, 2008, pp. 1–8.
- [7] S. Buzzi, M. Lops and L. Venturino Track-before-detect procedures for early detection of moving target from airborne radars *IEEE Trans. Aerosp. Electron. Syst.*, vol. 41, no. 3, pp. 937–954, Jul. 2005, doi: [10.1109/TAES.2005.1541440](https://doi.org/10.1109/TAES.2005.1541440).
- [8] H. Im and T. Kim Optimization of multiframe target detection schemes *IEEE Trans. Aerosp. Electron. Syst.*, vol. 35, no. 1, pp. 176–187, Jan. 1999, doi: [10.1109/7.745690](https://doi.org/10.1109/7.745690).
- [9] M. G. S. Bruno and J. M. F. Moura Optimal multiframe detection and tracking in digital image sequences In *Proc. IEEE Int. Conf. Acoust. Speech Signal Process.*, Istanbul, Turkey, 2000, pp. 3192–3195.
- [10] Y. Barniv Dynamic Programming Solution for Detecting Dim Moving Targets *IEEE Trans. Aerosp. Electron. Syst.*, vol. AES-21, no. 1, pp. 144–156, Jan. 1985, doi: [10.1109/TAES.1985.310548](https://doi.org/10.1109/TAES.1985.310548).
- [11] J. Arnold, S. W. Shaw and H. Pasternack Efficient target tracking using dynamic programming *IEEE Trans. Aerosp. Electron. Syst.*, vol. 29, no. 1, pp. 44–56, Jan. 1993, doi: [10.1109/7.249112](https://doi.org/10.1109/7.249112).
- [12] W. Li, W. Yi, M. Wen and D. Orlando Multi-PRF and multi-frame track-before-detect algorithm in multiple PRF radar system *Signal Process.*, vol. 174, p. 107648, Sep. 2020, doi: [10.1016/j.sigpro.2020.107648](https://doi.org/10.1016/j.sigpro.2020.107648).
- [13] D. J. Salmond and H. Birch A particle filter for track-before-detect In *Proc. Am. Control Conf.*, Arlington, VA, USA, 2001, pp. 3755–3760.
- [14] B. -N. Vo, B. -T. Vo, N. -T. Pham and D. Suter Joint Detection and Estimation of Multiple Objects From Image Observations *IEEE Trans. Signal Process.*, vol. 58, no. 10, pp. 5129–5141, Oct. 2010, doi: [10.1109/TSP.2010.2050482](https://doi.org/10.1109/TSP.2010.2050482).
- [15] P. Uruski and M. Sankowski On estimation of performance of track-before-detect algorithm for 3D stacked-beam radar In *Proc. Int. Conf. Microw., Radar, Wireless Commun.*, Warsaw, Poland, 2004, pp. 97–100.
- [16] B. D. Carlson, E. D. Evans and S. L. Wilson Search radar detection and track with the Hough transform. Part II: detection statistics *IEEE Trans. Aerosp. Electron. Syst.*, vol. 30, no. 1, pp. 109–115, Jan. 1994, doi: [10.1109/7.250411](https://doi.org/10.1109/7.250411).
- [17] D. Orlando, F. Ehlers and G. Ricci Track-before-detect algorithms for bistatic sonars In *Proc. Int. Workshop Cognitive Inf. Process.*, Elba, Italy, 2010, pp. 180–185.
- [18] E. Grossi, M. Lops and L. Venturino A Novel Dynamic Programming Algorithm for Track-Before-Detect in Radar Systems *IEEE Trans. Signal Process.*, vol. 61, no. 10, pp. 2608–2619, May 2013, doi: [10.1109/TSP.2013.2251338](https://doi.org/10.1109/TSP.2013.2251338).
- [19] S.-W. Yeom, T. Kirubarajan and Y. Bar-Shalom Track segment association, fine-step IMM and initialization with Doppler

- for improved track performance *IEEE Trans. Aerosp. Electron. Syst.*, vol. 40, no. 1, pp. 293–309, Jan. 2004, doi: [10.1109/TAES.2004.1292161](https://doi.org/10.1109/TAES.2004.1292161).
- [20] F. Kural, F. Ankan, O. Arıkan and M. Efe Incorporating Doppler Velocity Measurement for Track Initiation and Maintenance In *Proc. IEE Seminar Target Tracking Algorithms Appl.*, Birmingham, AL, USA, 2006, pp. 107–114.
- [21] D. Mušicki, T. L. Song, H. H. Lee and D. Nešić Correlated Doppler-assisted target tracking in clutter *IET Radar, Sonar Navig.*, vol. 7, no. 1, pp. 94–100, Jan. 2013, doi: [10.1049/iet-rsn.2012.0115](https://doi.org/10.1049/iet-rsn.2012.0115).
- [22] C. Gao, J. Yan, X. Peng, B. Chen and H. Liu Intelligent multiframe detection aided by Doppler information and a deep neural network *Inf. Sci.*, vol. 593, pp. 432–448, May 2022, doi: [10.1016/j.ins.2022.01.029](https://doi.org/10.1016/j.ins.2022.01.029).
- [23] Y. Bar-Shalom *Tracking and data association*. San Diego, CA, USA: Academic Press Professional, Inc., 1987.
- [24] W. Xiong, Y. Lu, J. Song and X. Chen A Two-Stage Track-before-Detect Method for Non-Cooperative Bistatic Radar Based on Deep Learning *Remote Sens.*, vol. 15, no. 15, p. 3757, Jul. 2023, doi: [10.3390/rs15153757](https://doi.org/10.3390/rs15153757).
- [25] Y. Chen, Y. Wang, F. Qu and W. Li A Graph-Based Track-Before-Detect Algorithm for Automotive Radar Target Detection *IEEE Sens. J.*, vol. 21, no. 5, pp. 6587–6599, Mar. 2021, doi: [10.1109/JSEN.2020.3042079](https://doi.org/10.1109/JSEN.2020.3042079).
- [26] F. Scarselli, M. Gori, A. C. Tsoi, M. Hagenbuchner and G. Monfardini The Graph Neural Network Model *IEEE Trans. Neural Netw.*, vol. 20, no. 1, pp. 61–80, Jan. 2009, doi: [10.1109/TNN.2008.2005605](https://doi.org/10.1109/TNN.2008.2005605).
- [27] L. Wu, Y. Chen, K. Shen, X. Guo, H. Gao, S. Li, J. Pei and B. Long *Graph Neural Networks for Natural Language Processing: A Survey*. Norwell, MA, USA: Now Publishers Inc., 2023.
- [28] Z. Wu, S. Pan, F. Chen, G. Long, C. Zhang and P. S. Yu A Comprehensive Survey on Graph Neural Networks *IEEE Trans. Neural Netw. Learn. Syst.*, vol. 32, no. 1, pp. 4–24, Jan. 2021, doi: [10.1109/TNNLS.2020.2978386](https://doi.org/10.1109/TNNLS.2020.2978386).
- [29] J. Zhou, G. Cui, S. Hu, Z. Zhang, C. Yang, Z. Liu, L. Wang, C. Li and M. Sun, Graph Neural Networks: A Review of Methods and Applications *AI Open*, vol. 1, pp. 57–81, Sep. 2020, doi: [10.1016/j.aiopen.2021.01.001](https://doi.org/10.1016/j.aiopen.2021.01.001).
- [30] A. Scotti, N. N. Moghadam, D. Liu, K. Gafvert and J. Huang, Graph Neural Networks for Massive MIMO Detection 2020, *arXiv:2007.05703v1*.
- [31] F. Fent, P. Bauerschmidt and M. Lienkamp RadarGNN: Transformation Invariant Graph Neural Network for Radar-based Perception In *Proc. IEEE Conf. Comput. Vis. Pattern Recognit. Workshops*, Vancouver, BC, Canada, 2023, pp. 182–191.
- [32] N. Su, X. Chen, J. Guan, Y. Huang, X. Wang and Y. Xue Radar Maritime Target Detection via Spatial–Temporal Feature Attention Graph Convolutional Network *IEEE Trans. Geosci. Remote Sens.*, vol. 62, no. 5102615, pp. 1–15, Jan. 2024, doi: [10.1109/TGRS.2024.3358862](https://doi.org/10.1109/TGRS.2024.3358862).
- [33] C. Gao, J. Yan, B. Chen, P. K. Varshney, T. Jia and H. Liu Data association for maneuvering targets through a combined siamese network and XGBoost model *Signal Process.*, vol. 211, no. 109086, pp. 1–12, Oct. 2023, doi: [10.1016/j.sigpro.2023.109086](https://doi.org/10.1016/j.sigpro.2023.109086).
- [34] B. P. Chamberlain, S. Shirobokov, E. Rossi, F. Frasca, T. Markovich, N. Y. Hammerla, M. M. Bronstein and M. Hansmire Graph Neural Networks for Link Prediction with Subgraph Sketching In *Int. Conf. Learn. Representations*, Kigali, Rwanda, 2023, pp. 1–27.
- [35] M. Gao, P. Jiao, R. Lu, H. Wu, Y. Wang and Z. Zhao Inductive Link Prediction via Interactive Learning Across Relations in Multiplex Networks *IEEE Trans. Comput. Social Syst.*, vol. 11, no. 3, pp. 3118–3130, Jun. 2024, doi: [10.1109/TCSS.2022.3176928](https://doi.org/10.1109/TCSS.2022.3176928).
- [36] B. Labbé, R. Héroult and C. Chatelain Learning Deep Neural Networks for High Dimensional Output Problems In *Proc. Int. Conf. Mach. Learn. Appl.*, Miami, FL, USA, 2009, pp. 63–68.
- [37] D. Gaifulina and I. Kotenko Selection of Deep Neural Network Models for IoT Anomaly Detection Experiments In *Proc. Euromicro Int. Conf. Parallel, Distrib. Network-Based Process.*, Valladolid, Spain, 2021, pp. 260–265.
- [38] J. Gilmer, S. S. Schoenholz, P. F. Riley, O. Vinyals and G. E. Dahl Neural message passing for Quantum chemistry In *Proc. Int. Con. Mach. Learn.*, Sydney, NSW, Australia, 2017, pp. 1263–1272.
- [39] P. Veličković, G. Cucurull, A. Casanova, A. Romero, P. Liò and Y. Bengio Graph Attention Networks In *Int. Conf. Learn. Representations*, Vancouver, CANADA, 2018, pp. 1–12.
- [40] S. Brody, U. Alon and E. Yahav How Attentive are Graph Attention Networks? In *Int. Conf. Learn. Representations*, Virtual, 2022, pp. 1–26.
- [41] P. H. C. Avelar, A. R. Tavares, T. L. T. da Silveira, C. R. Jung and L. C. Lamb Superpixel Image Classification with Graph Attention Networks In *Proc. SIBGRAPI Conf. Graph., Patterns Imag.*, Porto de Galinhas, Brazil, 2020, pp. 203–209.
- [42] Q. Li, Y. Shang, X. Qiao and W. Dai Heterogeneous Dynamic Graph Attention Network In *Proc. IEEE Int. Conf. Knowl. Graph*, Nanjing, China, 2020, pp. 404–411.
- [43] I. Goodfellow, Y. Bengio and A. Courville *Deep Learning*. Cambridge, MA, USA: MIT Press, 2016.
- [44] B. Ristic, B. -N. Vo, D. Clark and B. -T. Vo A Metric for Performance Evaluation of Multi-Target Tracking Algorithms *IEEE Trans. Signal Process.*, vol. 59, no. 7, pp. 3452–3457, Jul. 2011, doi: [10.1109/TSP.2011.2140111](https://doi.org/10.1109/TSP.2011.2140111).
- [45] D. Schuhmacher, B. -T. Vo and B. -N. Vo A Consistent Metric for Performance Evaluation of Multi-Object Filters *IEEE Trans. Signal Process.*, vol. 56, no. 8, pp. 3447–3457, Aug. 2008, doi: [10.1109/TSP.2008.920469](https://doi.org/10.1109/TSP.2008.920469).
- [46] M. Ancona, E. Ceolini, A. C. Öztireli and M. Gross A unified view of gradient-based attribution methods for Deep Neural Networks In *NIPS Workshop Interpreting, Explaining, Visualizing Deep Learn.*, Long Beach, CA, USA, 2017, pp. 1–11.
- [47] L. Breiman Random Forests *Mach. Learn.*, vol. 45, pp. 5–32, Oct. 2001, doi: [10.1023/A:1010933404324](https://doi.org/10.1023/A:1010933404324).
- [48] F. K. Ewald, L. Bothmann, M. N. Wright, B. Bischl, G. Casalicchio and G. König A Guide to Feature Importance Methods for Scientific Inference 2024, *arXiv:2404.12862*.
- [49] N. J. Cox Speaking Stata: Creating and Varying Box Plots *Stata J.*, vol. 9, no. 3, pp. 478–496, Sep. 2009, doi: [10.1177/1536867X0900900309](https://doi.org/10.1177/1536867X0900900309).